THE JOURNAL OF COMPARATIVE NEUROLOGY 488:320–330 (2005)

Connection from Cortical Area V2 to V3A in Macaque Monkey

JOHN C. ANDERSON[1,2]* AND KEVAN A.C. MARTIN[1,2]
[1]Institute for Neuroinformatics, University of Zürich, 8057 Zürich, Switzerland
[2]Eidgenossiche Technische Hochschule Zürich, 8057 Zürich, Switzerland

ABSTRACT

The V2 projection to V3A was labeled by pressure microinjecting biotinylated dextran amine (BDA) and *Phaseolus vulgaris* lectin (PHA-L) into V2 just posterior to the lunate sulcus. Dense terminal labeling in clusters was found in layer 4, with a weaker terminal projection in layer 3. About 3.5–4.1% of the synapses in the densest bouton clusters in layer 4 were made by labeled boutons. All were asymmetric (Gray's type 1) synapses, made by spiny, excitatory neurons. The most frequently encountered synaptic targets were spines (76% in layer 4, 98% in layer 2/3). The remainder of the synaptic targets were dendritic shafts, of which just less than half (44%) had the characteristic ultrastructure of smooth (inhibitory) cells. Multisynaptic boutons were rare (mean synapses per bouton for layer 4 1.2, for layer 2/3 1.1). The mean size of the postsynaptic densities found on spines (0.11 μm^2) was not significantly different from that for dendrites (0.09 μm^2). In terms of their type, laminar location, number, and targets, the synapses that formed the V2 projection to V3A are typical of a major, excitatory, feedforward projection of macaque visual cortex. J. Comp. Neurol. 488: 320–330, 2005.

Indexing terms: visual cortex; area V3A; corticocortical; light and electron microscopy; synapse morphology; postsynaptic target

In studies of visual processing in extrastriate cortex in the monkey, the areas V2, V4, and MT (V5) have received the most intense scrutiny. An early study by Zeki (1978a) in macaque showed that, in the proportions of orientation and motion selective cells, V3A was indistinguishable from V2, V3, and V4. Area V4 stood out by having large numbers of color-sensitive cells, whereas MT was prominent because of its large numbers of direction-selective cells. With the development of functional imaging, one of the areas that emerges with some prominence in imaging studies in both humans and monkeys is V3A, which shows strong activation with motion and depth stimuli and has high contrast sensitivity (Tootell et al., 1997; Backus et al., 2001; Tsao et al., 2003). In humans, the functional magnetic resonance imaging (fMRI) data indicate that V3A appears to be more sensitive to motion than in monkeys (Tootell et al., 1997; Orban et al., 2003).

There are relatively few single-unit studies of V3A in the macaque. With anesthetized monkeys, Gaska et al. (1988) found that the spatial frequency tuning was similar to that of V1 neurons for the same eccentricity and that the temporal frequency tuning was low-pass. These properties led them to suppose that V3A forms part of the ventral pathway to V4 and inferotemporal cortex. Against this, Zeki (1978a) noted that V3A neurons have no color sensitivity, suggesting rather a role in the dorsal stream to parietal cortex. Indeed, Galletti and Battaglini (1989) found neurons in V3A of behaving monkeys whose responses were modulated by eye position. Nakamura and Colby (2000, 2002) also emphasized the role of V3A neurons in coordinate transformations for retinal and eye position. In addition, some neurons carried memory- and saccade-related signals. Attention and expectation of reward modulate the responses of V3A neurons (Thiele et al., 1999; Nakamura and Colby, 2000).

Area V3A is richly connected to surrounding cortical areas and also makes reciprocal connections with frontal eye fields (Schall et al., 1995; Stanton et al., 1995). It receives feedforward connections from caudal cortical areas, including a sparse connection from V1 (Zeki, 1978b; Van Essen et al., 1986), and a strong input from V2 (Gat-

Grant sponsor: European Union; Grant number: QULG3-1999-01064 (to K.A.C.M.); Grant sponsor: Human Frontier Science Program; Grant number: RG0123/2000-B (to K.A.C.M.); Grant sponsor: Swiss National Science Foundation (to K.A.C.M.).

*Correspondence to: John C. Anderson, Institute for Neuroinformatics, University of Zürich and ETH Zürich, Winterthurerstr. 190, 8057 Zürich, Switzerland. E-mail: jca@ini.phys.ethz.ch

Received 13 July 2004; Revised 24 January 2005; Accepted 16 February 2005

DOI 10.1002/cne.20580

Published online in Wiley InterScience (www.interscience.wiley.com).

tass et al., 1997) and V3 (Felleman et al., 1997). If V1 is cooled, V3 stops responding to visual stimulation, but many neurons in V3A continue responding (Girard et al., 1991). After V1 inactivation, residual activity is found in MT, to which V3A is reciprocally connected (Girard et al., 1991). In addition to MT in the dorsal stream, V3A is also connected to lateral intraparietal area (LIP; Cavada and Goldman-Rakic, 1989; Andersen et al., 1990; Blatt et al., 1990, Morel and Bullier, 1990, Baizer et al., 1991; Nakamura et al., 2001), dorsal prelunate area (Andersen et al., 1990), medial superior temporal area (MST; Boussaoud et al., 1990), and fundus of the superior temporal visual area (FST; Boussaoud et al., 1990) and the parietooccipital area (PO; Colby et al., 1988; Shipp et al., 1998). V3A also has reciprocal connections to areas of the ventral stream, including ventral posterior area (VP, Felleman et al., 1997), V4 (Felleman and Van Essen 1983), and TEO (Morel and Bullier, 1990; Webster et al., 1994).

From both physiological and anatomical evidence, it is clear that V3A lies at a key crossroads in the extrastriate circuit. Surprisingly, however, nothing is known of the synaptic profile of any input to V3A. In the present study, we examined quantitatively the synapses formed in V3A by one of its major feedforward inputs, that arising in V2, and provide comparisons, where possible, with other quantitative electron microscopic studies of projections in extrastriate cortex.

MATERIALS AND METHODS

The material presented here was taken from two adult female macaque monkeys (*Macaca mulatta*). Animal treatment and surgical protocols were carried out in accordance with the guidelines of the Kantonales Veterinaeramt of Zürich. The projection from V2 to MT in these same two animals has been described (Anderson and Martin, 2002), and the following procedures are identical. Animals were prepared for surgery after the administration of an intramuscular premedication of xylazine (Rompun; Beyelar; 0.5 mg/kg)/ketamine (Ketalar; Parke Davis; 10 mg/kg). This was followed by cannulation of a femoral vein for the delivery of alphaxalone/alphadalone (Saffan; Glaxo) to establish complete anesthesia.

Each animal received pressure injections (~0.5 μl each) of the neuronal tracers biotinylated dextran amine (BDA; Molecular Probes, Leiden, The Netherlands) and *Phaseolus vulgaris* leucoagglutinen (PHA-L; Vector Laboratories, Burlingame, CA). One animal received four injections of 10% BDA in 0.01 M phosphate-buffered saline (PBS), pH 7.4, and two of PHA-L in 10 nM phosphate buffer (PB), pH 7.4. The second animal received five injections of BDA and three injections of PHA-L. Both tracers were used in order to assess their relative merits in a study of this type. The tracers were injected into area V2 (area 18) along the crest of the lunate gyrus (see, e.g., Anderson and Martin, 2002; see Fig. 1). With one exception, needle tracks were all confined to the gray matter of V2, and the label could be followed through all laminae. In one animal, the injections were made into the dorsal surface of V2, the needle track being almost parallel to the cortical laminae. Penetrations made in the second animal traversed the tip of the gyrus and extended into the lunate sulcus (see, e.g., Anderson and Martin, 2002; see Fig. 1B). One track in this animal went through the white matter.

After a 14-day survival period, anesthesia was again induced with ketamin/xylazine, and the monkeys were deeply anesthetized with i.v. pentobarbital (20 mg/kg) and immediately perfused transcardially with a normal saline solution, followed by a solution of 4% paraformaldehyde, 0.3% gluteraldehyde, and 15% picric acid in 0.1 M PB, pH 7.4. The brain was removed from the skull, and a block of cortex containing the injection site and area V3A was removed. The block was allowed to sink in sucrose solutions of 10%, 20%, and 30% in 0.1 M PB. Sections were cut from the block at 80 μm in the parasagittal plane and collected in 30% sucrose in 0.1 M PB. The sections were then freeze-thawed in liquid nitrogen and washed in 0.1 M PB. We used standard procedures to reveal the neuronal tracers. In brief outline; washes in PBS were followed by 10% normal swine serum (NSS) in PBS (1 hour). The biotinylated antibody to PHA-L was diluted in the above at 1:200 and exposed for 48 hours at 5°C. Further washes in NSS preceded overnight exposure (5°C) to an avidin-biotin complex (Vector ABC Elite Kit), which precludes the need for a secondary antibody. The peroxidase activity was identified by using 3,3-diaminobenzidene tetrahydrochloride (DAB). After assessment by light microscopy (LM) selected regions of tissue were treated with 1% osmium tetroxide in 0.1 M PB. Dehydration through alcohols (1% uranyl acetate in the 70% alcohol) and propylene oxide allowed flat mounting in Durcupan (Fluka) on glass slides.

LM observations of labeled axons were carried out to locate and select regions of interest for electron microscopy (EM). We reconstructed individual collaterals in the less densely innervated areas for correlated LM and EM. Serial ultrathin sections were collected at 70 nm thickness on Pioloform-coated single-slot copper grids. Labeled boutons were photographed at a magnification of ×21,000. Synapses and associated structures were classified by using conventional criteria. Collections of serial sections were digitized and reconstructed using Trakem, an in-house EM digitization package. To measure and display the postsynaptic densities of labeled boutons, we used software developed by ourselves, which has been described in outline elsewhere (see Materials and Methods in Anderson et al., 1998).

The estimates of labeled bouton density were derived using the physical disector method (Sterio, 1984). We selected regions that were densely innervated by labeled axon for reembedding. Serial 70-nm-thick sections were collected from these regions, and a reference section and a look-up section were selected. The reference and look-up sections were separated by one section. Photographs were taken with the electron microscope to form patches of tissue, e.g., 2 × 8 images. All electron micrographs were taken at ×11,500. Synapses that were in the reference section but that disappeared in the look-up section were counted. Synapses that were present in both look-up and reference sections were not counted (Sterio, 1984). Adobe Photoshop CS and Adobe Illustrator CS were used to prepare digital photomicrographs and enhance image contrast.

RESULTS

LM

The pressure injections into V2 immediately posterior to the lunate sulcus resulted in label spread over 5–7 mm

mediolaterally. BDA labeling was poor at the injection site, but PHA-L labeling was excellent. From this we assume that the axons seen in V3A were labeled with PHA-L. Labeling was densest along the path of the penetrations. Most of the uptake was by pyramidal cells of layer 2/3, covering most of the tip of the gyrus, but labeled cell bodies were also found in all other layers. Strong anterograde labeling was seen in striate and extrastriate visual areas, including V1, V3A, and V5, along with some pale retrogradely stained cell bodies. The strongest transport was to V1, where the retrograde labeling was similar to that previously reported by Kennedy and Bullier (1985), i.e., predominantly in layers 2/3 and 4B, with some sparse cell bodies scattered along the layer 5–6 border. No cell or terminal labeling was evident in layer 4 of V1. The border between areas V3 and V3A was identified as the axon clustering found in the lunate sulcus (Felleman et al., 1997; Fig. 6B), in one case in the fundus and in the other case in the anterior bank of the lunate sulcus (Fig. 1).

Beck and Kaas (1999) consider V3 and V3A to be part of a single dorsomedial visual area, identified anatomically by its dense myelin staining. Despite the fact that the osmium gave excellent staining of myelin, we were unable to distinguish V3A from surrounding areas on the basis of differences in myelin staining. The border between these two visual areas, V3 and V3A, represents the vertical meridian (Adams and Zeki, 2001). Because of the retinotopic correspondence in connections, we expected to see labeled axons close to the representation of the vertical meridian at the V3–V3A border, where the labeled axons were indeed found. No labeling was seen at the V2–V3 border, where the horizontal meridian is represented.

In area V3A, the labeled axons entered from the white matter. On reaching layer 4, most of the axons branched extensively and formed synaptic boutons (Fig. 2). Layer 4 was identified by dark staining in the osmicated material and by a dense granular appearance in the Nissl-stained material. These features also coincided with the highest density of labeled terminations. Labeled axons (>0.5 μm) traversed extensively within layer 4. Seen in EM, many axons possessed a thick coating of myelin. This profusion of myelinated axons, fine bouton-bearing axons, and both en passant and terminaux boutons gave an overall patchy appearance to the innervation site of one animal when viewed at low power in the light microscope. However, this patchiness was less distinct that that seen in area V5 or MT in the same material (see Anderson and Martin, 2002; Fig. 2). In the second animal, the axon labeling in layer 4 was confined to the fundus of the sulcus, adjacent to labeling in area V3 (Fig. 1).

Axons that projected into the more superficial layers were more slender than the main trunks seen in layer 4. They gave rise to mostly en passant boutons of a fairly uniform size spaced at fairly regular intervals. Most of these axons terminated in or before upper layer 2/3. Occasionally, thicker axons, passing through layer 3, branched before reaching layer 2 and produced a radially aligned, fanlike arborization. The axon diameter in these superficial layer axons was reduced rapidly as they branched.

Weak retrograde labeling was evident as palely stained neuronal somata and proximal dendrites, in some instances. These cells were sparse and were clearly of a pyramidal morphology. The majority of retrogradely labeled somata occurred in layer 2/3, occasionally in layer 6.

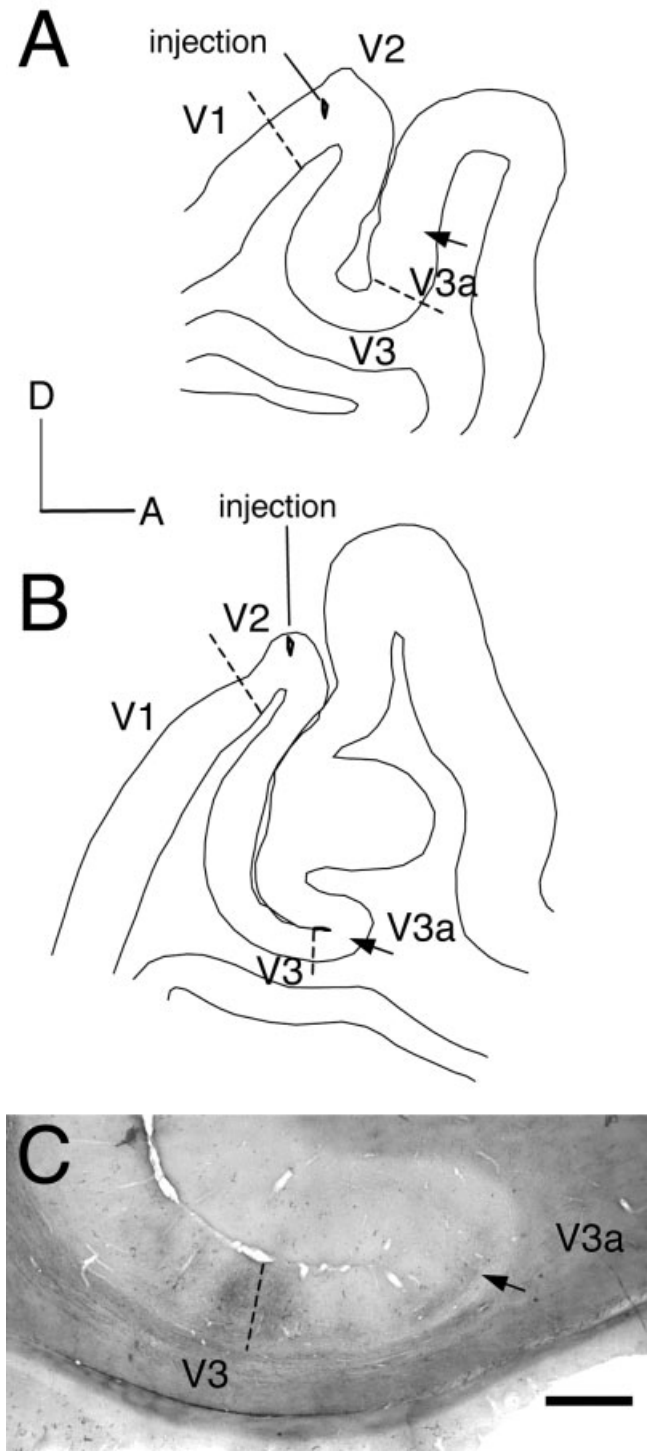

Fig. 1. Drawings of two parasagittal sections (**A,B**) from macaque brain and a photomicrograph (**C**) from one of these sections. Indicated are region in which injections were made along the edge of the lunate sulcus and the region from which labeled axons were sampled for electron microscopic analysis (arrows). The borders between visual areas are indicated by a dashed line. D, dorsal; A, anterior. Scale bar = 1 mm.

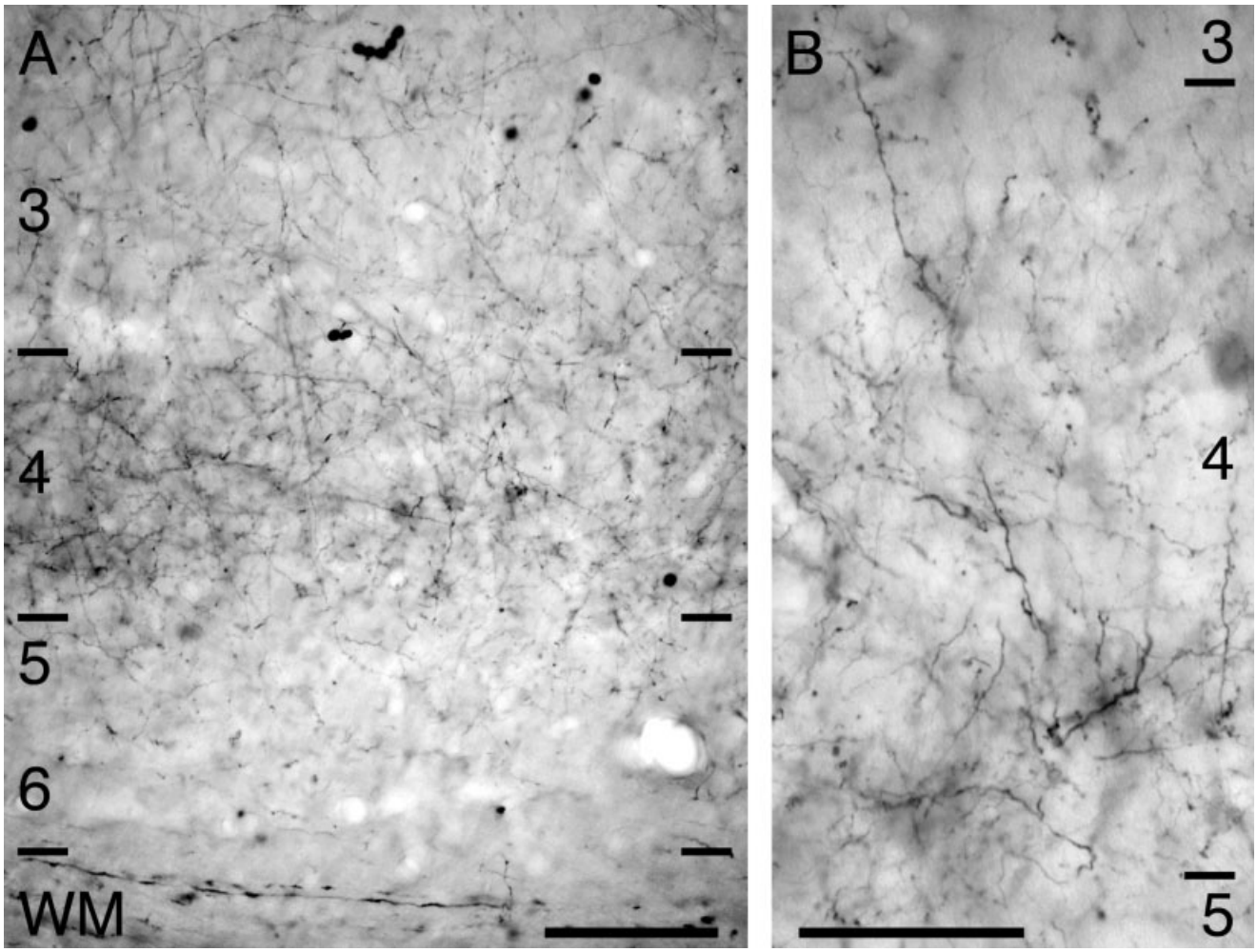

Fig. 2. Light micrographs of cortical area V3A showing PHA-L-labeled axon termination zone. **A:** Labeled terminals form dense band in layer 4 and lesser projections into layer 3. Laminae and their boundaries are indicated to the left and right. **B:** Section from a second monkey at higher magnification. The labeled fibers branch profusely in layer 4 to form a dense network of axon collaterals and terminals. Laminae and their boundaries are indicated at right. Scale bars = 0.1 mm in A; 50 μm in B.

One spiny stellate cell and one star pyramidal cell were found within the cloud of axons near the layer 3–4 border. The density of the labeling in layer 4 made it impossible to reconstruct at LM level extensive portions of single axons. This density also made tight LM/EM correlation impossible. Thus, we selected for EM analysis areas of layer 4 with the densest labeling as determined in the light microscope. The projections to the superficial layers were sparser, and this enabled us to correlate LM and EM.

EM

We sampled a total of 106 boutons from layers 2/3 and 4 (48 from layer 2/3 and 58 from layer 4). All were serially sectioned and completely reconstructed. In total, 120 labeled synapses were examined, all of which were asymmetric (Gray's type 1). We reproduce the electron micrographs of boutons in this study at approximately the same magnification as the images used in previous studies of V1 and V2 afferent boutons in MT (Anderson et al., 1998; Anderson and Martin, 2002), to facilitate a comparison with other corticocortical projections we have studied in the macaque.

The reaction end product was dark, though of variable intensity, in different boutons. Vesicles and mitochondria were clearly visible inside the boutons, and the synaptic clefts were not obscured by label. Myelinated axons were also labeled, confirming that the antibody had penetrated well, despite the insulating sheath. Some axons were myelinated right up to the synaptic bouton. Most boutons were small (~0.5 μm diameter), compact structures containing one or two mitochondria and a cluster of vesicles over the region of the synaptic specialization (see, e.g., Figs. 3, 4). The synapse was indicated by the presence of presynaptic vesicles, a synaptic cleft, and a postsynaptic density in the target structure. Occasionally, we saw a density within the labeled bouton that was mirrored by a similar density within the target. In the immediate vicinity of the presynaptic density, there were no vesicles. This mirror-like configuration was always seen close or adjacent to a conventional asymmetric synapse and was clas-

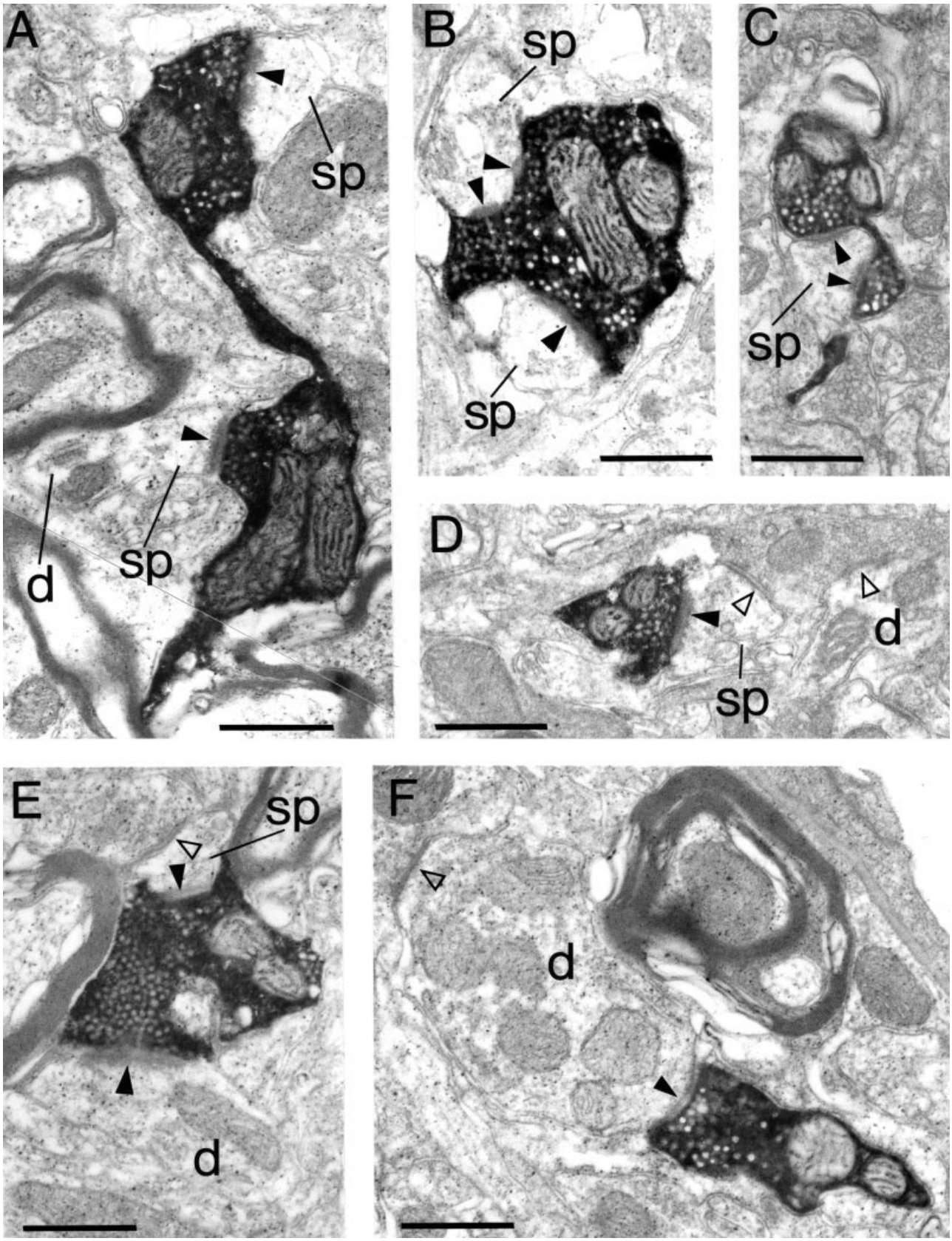

Figure 3

sified as a puncta adherens (Peters et al., 1991). We did not include these puncta in our reconstructions or estimates and measurements of synapses.

Spines. Serially sectioning the bouton, synapse, and target structures greatly assisted in determining the type of target that formed synapses with the labeled boutons. We also used standard ultrastructural criteria to classify targets (Peters et al., 1991). The most frequent targets were small spines (Figs. 3, 4). Occasionally, we were able to trace spines back to a parent dendrite (Figs. 3A, 4E). A second synapse from an unlabeled bouton was seen on five spines and in all cases was of a symmetric morphology (Gray's type 2). All five dual-input spines were located in layer 4 (Fig. 3D,E). Spine synapses formed 52 of the 53 synapses examined in layer 2/3 and 51 of the 67 synapses identified in layer 4.

Boutons sometimes had the target spine or part of the spine embedded within the bouton (Figs. 3C, 4B,C,E). We have previously reported similar observations in the case of the V1 afferent boutons in MT. The synapses in MT were complex, highly perforated, and extensive (see Fig. 8 in Anderson et al., 1998). The synapses in V3A were not as complex as those found on V1 boutons in MT but were quite extensive and often covered a large part of the spine that was embedded or "pinched" into the bouton (Figs. 3C, 4B,C,E).

Dendrites. Dendrites were also the targets of labeled boutons. These were usually identified by reconstruction from serial sections or in individual sections by the presence of mitochondria and microtubules. Most dendrites were about 0.5 μm diameter (Fig. 3E), the largest measuring ~0.9 μm diameter. Reconstructions of serial sections indicated that there were two basic classes of target dendrites. One class possessed spines and had dendritic shafts that showed little variation in diameter when reconstructed. The shaft formed few synapses, which is characteristic of the spiny dendrites of excitatory neurons (Fig. 3E). The sole dendritic synapse in layer 2/3 and 9 of 16 of the completely reconstructed synapses in layer 4 were formed with such spiny dendrites.

The other class of dendritic target had a morphology that differed markedly from that of the putative spiny dendrites. Such dendrites varied greatly in diameter in the serial reconstructions; they usually contained numerous mitochondria and, in single sections, could form multiple synapses with other unidentified boutons (Fig. 3F). These dendrites are quite characteristic of neurons with smooth, varicose dendrites that contain the inhibitory neurotransmitter γ-aminobutyric acid (GABA; Somogyi et al., 1983; Peters and Saint Marie, 1984; Kisvárday et al., 1985; Ahmed et al., 1997). A high proportion of serially reconstructed target dendrites in layer 4 had the features of smooth (putative GABAergic) neurons; 7 of 16 synapses (44%) formed on smooth dendrites. By comparison, smooth dendrites formed 26% of the dendritic targets of the V1 projection to MT and 52% of the dendritic targets of the V2 projection to MT (Anderson et al., 1998; Anderson and Martin, 2002).

Postsynaptic density. Reconstructing the bouton and its target gave us the opportunity to view the complete postsynaptic density as a 2-D or 3-D structure. We have used this technique previously to obtain values of the surface area of synapses (Anderson et el., 1998; Anderson and Martin, 2002). By focusing on the postsynaptic specialization rather than the presynaptic membrane, we avoided detail being obscured by the reaction end product in the bouton. The postsynaptic density can be perforated, giving it a doughnut or horseshoe morphology rather than that of a simple disc. Figures 5 and 6 show that the synapses with the more complex morphology are usually formed with spines.

The 2-D projection of all the postsynaptic densities is shown in Figures 5 and 6. There was little difference in the distributions of the areas of synapses made with the two main target types in layer 4, spines and dendrites ($P = 0.08$, two-tailed t-test). Spine synapses had a mean area of 0.11 μm^2 compared with 0.09 μm^2 for synapses with dendritic shafts. In comparisons of synapses from different laminae, the distributions overlapped considerably (Fig. 7). The layer 2/3 synapses (mean 0.110 μm^2, SEM 0.008) were not significantly different from those of layer 4 (mean 0.101 μm^2, SEM 0.006; $P = 0.4$, two-tailed t-test). The V2 boutons forming synapses with spines in layer 4 of areas V3a (mean 0.108 μm^2, SEM 0.007) and MT (mean 0.107 mm^2, SEM 0.01) were not significantly different ($P = 0.9$, two-tailed t-test). However, the spine synapses in layer 2/3 of V3a (mean 0.11 μm^2, SEM 0.008) were significantly larger than those in layer 2/3 of MT (mean 0.08 μm^2, SEM 0.005; $P = 0.005$, two-tailed t-test).

The mean size of the pooled synapses from V2 in layer 4 of V3A (mean 0.101 μm^2, SEM 0.006) was slightly less than that of the synapses of boutons from V2 in layer 4 of MT (mean 0.107 μm^2, SEM 0.008), but the differences were not significant ($P = 0.89$, two-tailed t-test). In single sections, some spines appeared to form two synapses with labeled boutons on opposite sides of the same spine head (Figs. 3C, 4B,E), but on reconstruction this proved to be a single synapse formed by a single bouton.

Target types. The most frequently encountered targets of V2 labeled boutons were spines. There was a dif-

Fig. 3. Electron micrographs of PHA-L-labeled electron-dense axon and boutons located in layer 4 of area V3A. A–D: Examples of synapses formed with spines. **A:** Two boutons en passant form asymmetric synapses (solid arrowheads) with spines (sp). One of the spines can be traced back to the small parent dendrite (d). Spines were the most frequent synaptic target seen in this study: small to medium-sized boutons targeted small spines, the labeled bouton containing at least one mitochondria, and the remaining space (usually above the synapse) is vesicle filled. **B:** Two spines (sp) form asymmetric synapses (solid arrowheads) with a labeled bouton. The postsynaptic density of the uppermost spine does not appear as a continuous structure but instead appears to be perforated or complex. This spine also contains a spine apparatus. **C:** A spine is partially embraced by a small labeled bouton that forms a perforated asymmetric synapse (solid arrowheads) with a spine (sp). **D:** A spine forms an asymmetric synapse (solid arrowhead) with a labeled bouton and a symmetric synapse (open arrowheads) with an unidentified bouton. The unidentified bouton also forms a symmetric synapse with a small dendrite (d). E,F: Examples of synapses formed with dendrites. **E:** A small-caliber dendrite (d) and a spine (sp) form asymmetric synapses (solid arrowheads) with a labeled bouton. Dendrites such as this containing few mitochondria, forming synapses infrequently, and showing little variation in diameter are characteristic of neurons with spiny dendrites. The spine also forms a symmetric synapse (open arrowhead) with an unidentified bouton. **F:** A large caliber dendrite (d) forms an asymmetric synapse (solid arrowhead) with a labeled bouton and a symmetric synapse (open arrowhead) with an unidentified bouton. The dendrite contains many mitocondria, forms many synapses, and has a beaded morphology. These features are characteristic of putative GABAergic neurons with smooth dendrites. Scale bars = 0.5 μm.

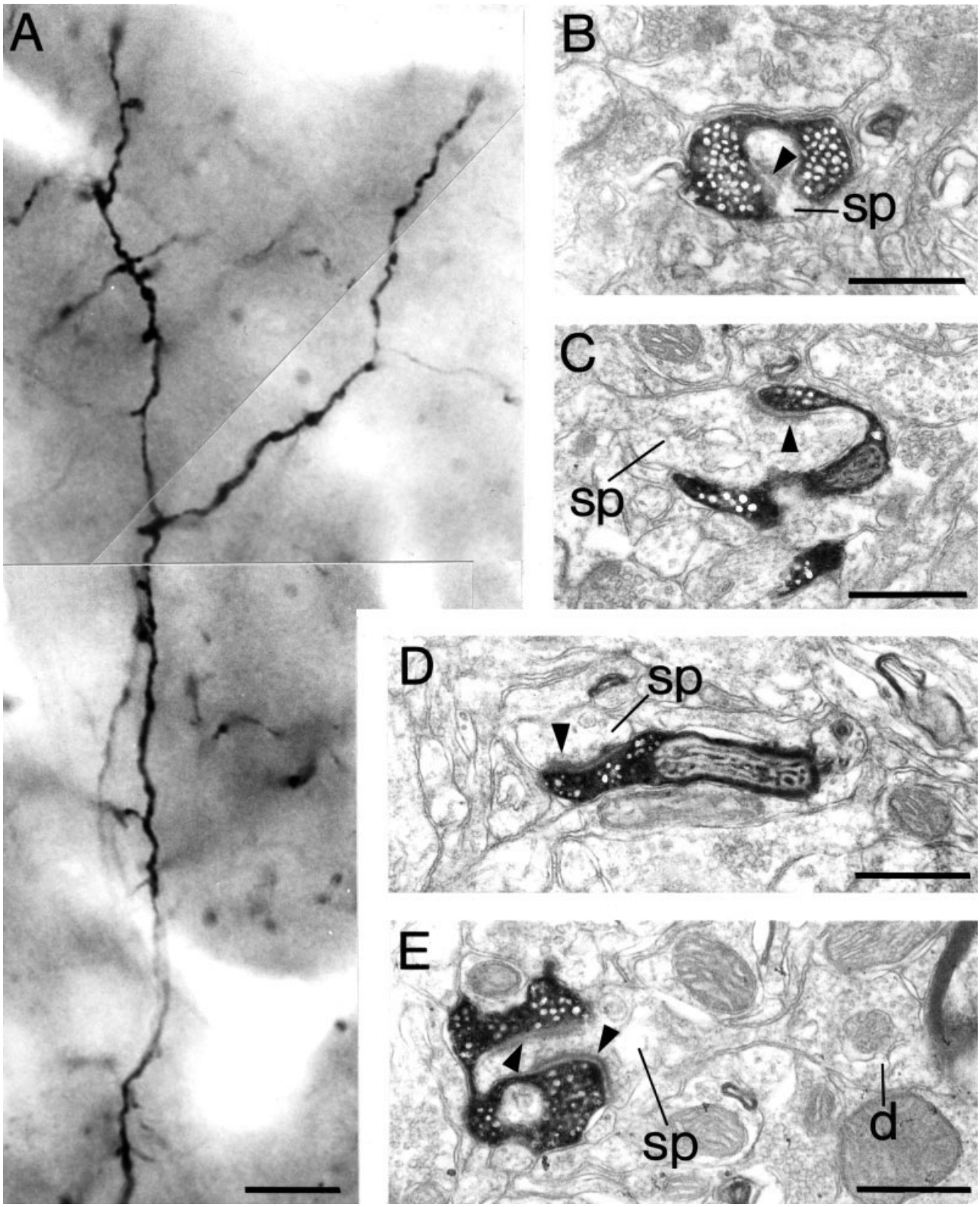

Fig. 4. Light and electron micrographs of PHA-L-labeled axon and boutons located in layer 2/3 of area V3A. **A:** Photomontage of an intensely labeled ascending collateral taken from layers 2 and 3. Numerous varicose swellings of the en passant and aux terminaux types can be clearly seen along the axon length. **B–E:** Electron micrographs of labeled boutons taken from the area between and inclusive of the branched collateral shown in A. Each bouton forms an asymmetric synapse (arrowheads) with a spine (sp). E: A labeled bouton forms an asymmetric synapse (arrowhead) with a spine. The spine can be traced back to the parent dendritic shaft (d). Scale bars = 10 μm in A; 0.5 μm in B–E.

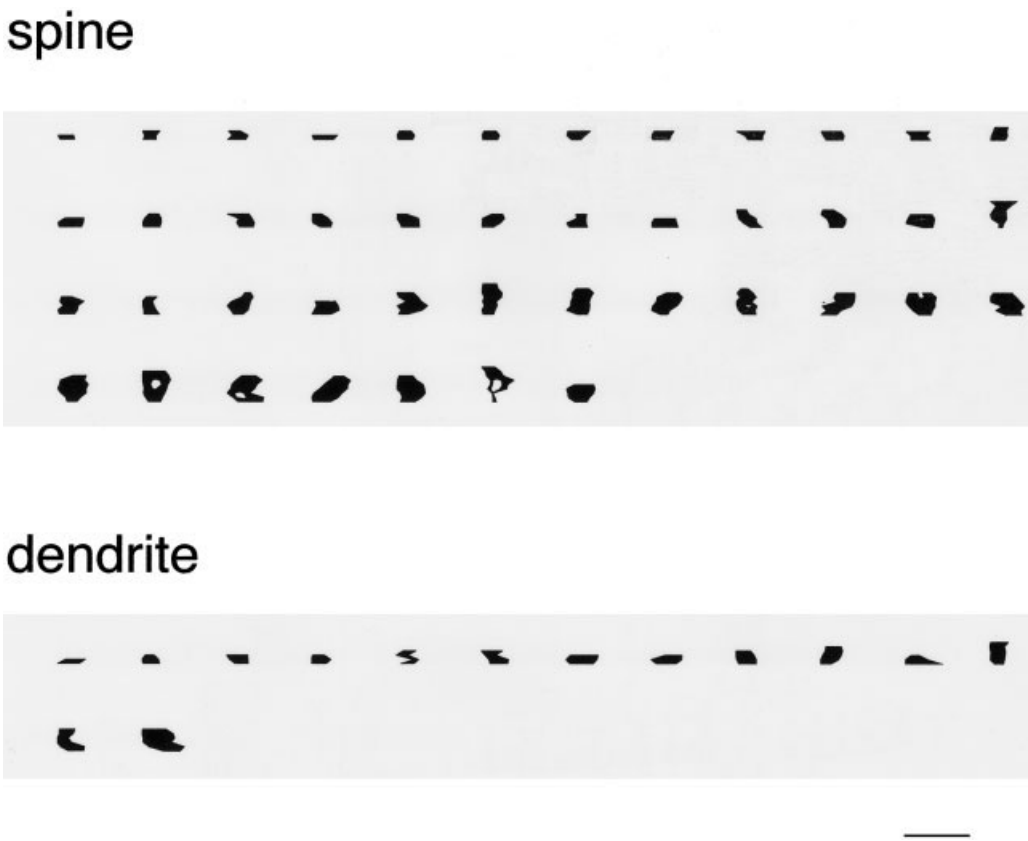

Fig. 5. Two-dimensional projection of the reconstructed postsynaptic densities found in layer 4 on spines and dendrites postsynaptic to labeled V2 boutons in area V3A. The densities are ordered by increasing surface area. Scale bar = 1 μm.

ference in the proportion of spines to dendrites as targets for the different laminae of innervation (Fig. 7). For this reason, we have not pooled the data from the two laminae. In layer 4, 76% of the labeled synapses were formed with spines and 24% with dendritic shafts, whereas, in layer 2/3, 98% of the synapses were formed with spines and 2% with dendritic shafts (Fig. 8).

As indicated above (see above under Dendrites), smooth neurons provided just under half of the dendritic shaft targets in layer 4. Serial reconstructions indicated that most boutons made only one synapse and only rarely more than two synapses (Fig. 9). On average, there were 1.1 and 1.2 synapses per labeled bouton in layers 2/3 and 4, respectively.

The same electron micrographs of labeled synaptic boutons and their targets were used to estimate the proportion of synapses formed with spines and dendrites in the neuropil of V3A. We found that, in layer 4 (n = 282) and layer 3 (n = 242), 63% and 86% of synapses, respectively, were formed with spines and the remainder with dendritic shafts. The dendritic profiles could be classed as either putative GABAergic smooth neurons or spiny neurons. We based our classification of the dendrites on serial reconstructions. For layers 4 and 3, we found 21% and 9%, respectively, of all targets to be putative GABAergic neurons (56% of dendrites in layer 4 and 60% in layer 3). We compared the labeled and nonlabeled synapses and the synapses of layer 3 and layer 4 by using a contingency table analysis. The proportions of targets of pooled layer 3 synapses were significantly different from those of pooled layer 4 targets ($P < 0.001$). Labeled and nonlabeled synapses from layer 4 showed no significant difference in the distribution of their target types ($P < 0.05$). The corresponding analysis for the targets of layer 3 synapses could not be performed because of low counts ($n < 5$) for labeled dendritic targets. The pooled data from labeled layers 3 and 4 was not significantly different from the pooled nonlabeled data from layers 3 and 4 ($P < 0.05$).

To estimate the relative proportion of synapses being contributed by V2 to area V3a, we made an unbiased stereological analysis of layer 4. We selected one section from each animal in which the labeling was particularly dense. In Figure 2 we show the terminal labeling in layer 4. We selected regions from within the densest patches of terminal innervation for our analysis with the unbiased disector method (Sterio, 1984). Although the blocks of tissue used for reembedding were selected from the densest zones of innervation, the distribution of labeled synapses in any ultrathin section could vary greatly. If the disector region was selected by using nonbiased features, such as the edge of the tissue or a scratch on the block face, we counted no labeled synapses. If we selected the location of the disector by finding a labeled bouton and then sam-

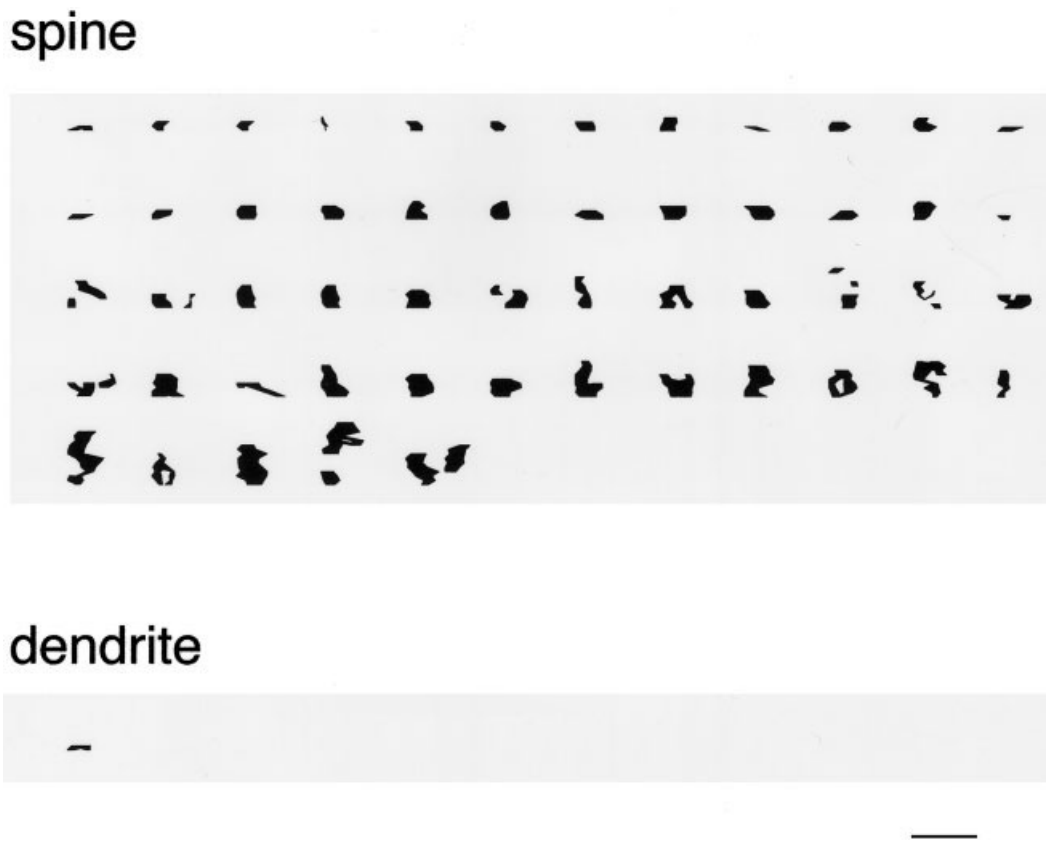

Fig. 6. Two-dimensional projection of the reconstructed postsynaptic densities found in layer 2/3 on spines and dendrites postsynaptic to labeled V2 boutons in area V3A. The densities are ordered by increasing surface area. Scale bar = 1 μm.

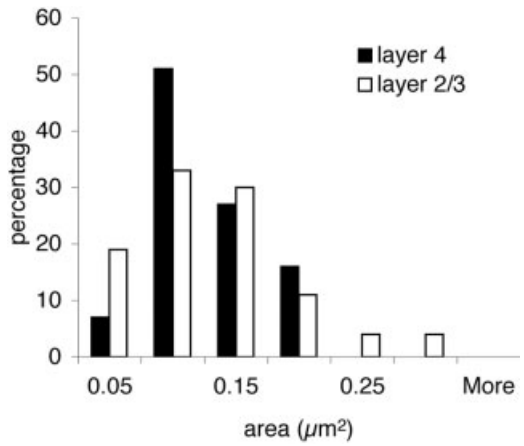

Fig. 7. Histogram of the distribution of postsynaptic areas (μm^2) formed by labeled V2 boutons in layers 2/3 (n = 54) and 4 (n = 46) of area V3A.

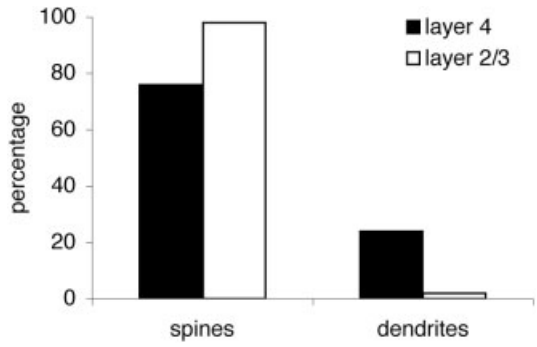

Fig. 8. Histogram of the synaptic targets of labeled V2 boutons in area V3A [for layer 2/3 (n = 53) and for layer 4 (n = 46)].

pling in the vicinity, we counted 3.5% (2 of 57) and 4.1% (7 of 169) of disappearing labeled synapses. This provides between two and six labeled V2 synapses per 10 × 10 × 10 μm cube of layer 4 in V3A.

DISCUSSION

We have shown that the projection from V2 to V3A, which is classified as "feedforward," forms asymmetric (excitatory) synapses principally with spiny (excitatory) neurons in layer 4, with a smaller projection almost exclusively to spiny neurons in layer 3. At the LM level, the terminal labeling in V3A was as strong as we have seen for any extrastriate projection we have studied (Anderson et al., 1998; Anderson and Martin, 2002). Counts of the

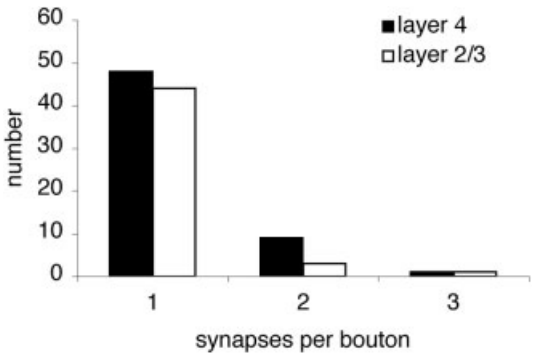

Fig. 9. Histogram of the number of synapses formed per labeled V2 bouton in layers 2/3 and 4 of area V3A.

identified synapses in the zones of densest labeling in layer 4 revealed that about 4% of the synapses originated from V2. This is similar to the proportion of labeled synapses found in layer 4 of MT after these same injections in V2 (Anderson and Martin, 2002). Both of these are comparable to the proportion of thalamic synapses in layer 4C of V1 (Latawiec et al., 2000) and slightly more than the 3% found for the projection from V1 to MT (Anderson et al., 1998). Thus the contribution of synapses from V2 to V3A is as numerous as any feedforword projection in primate visual cortex.

Rockland et al. (1999) estimated the contribution of pulvinocortical synapses in the lunate sulcus to be 0.18% of all excitatory synapses. Their estimate, based on LM observations in combination with ultrastructural data on V1 from other sources, may seem small compared with the 3–5% for the V2-V3A projection, but, as we have pointed out, the numbers are very location dependent. Our estimates are derived from the regions of high bouton density, whereas, if we select a region of layer 4 at random, the chances of finding even one labeled synapse are remote.

A feature of feedforward projections to layer 4, such as the thalamic projection to V1 or the V1 projection to V2 or the V2 projection to V3A and MT, is that they form segregated, stripe-like patches. For example, the ocular dominance stripes in the case of the thalamus, and the V1 projection segregates into thick, thin, and pale stripes seen in V2 after cytochrome oxidase staining. This tendency of the afferents to segregate themselves into mutually exclusive territories suggests that, in layer 4 at least, each stripe is an indication that only one afferent dominates the territory. Thus, in the case of the V2 projection to V3A, it is likely that no other area would form patches that overlap with the same stripes formed by the V2 projection. Instead, it is likely that a second projection would interdigitate in much the same way that thalamic afferents representing the left and right eyes do in V1. The second source of afferents is not known, but it must be another feedforward projection if it ends in layer 4. Because V3A appears early in the hierarchy of visual areas, the only possible candidates are V1 and V3. The projection from V1 is sparse (Zeki, 1978b; Van Essen et al., 1986), but, like the projection from V2 (Gattass et al., 1997), the projection from V3 is substantial (Felleman et al., 1997), and it is likely that it forms a feedforward projection to layer 4 that interdgitates with that from V2.

The mean surface area of synapses formed in layer 4 with spines was as large (0.101 μm^2) as the spine synapses formed by V2 axons in layer 4 of MT (0.107 μm^2; Anderson and Martin, 2002) but was smaller than those formed by V1 axons in layer 4 of MT (0.127 μm^2; Anderson et al., 1998). However, there was a large range in the size of the postsynaptic density for all projection synapses examined, both in MT and in V3A (see, e.g., Fig. 8 in Anderson et al., 1998; Fig. 8 in Anderson and Martin, 2002). In general, the largest synapses had a more elaborate shape than the simpler disk shape found for smaller synapses. The largest synapses are formed with spines, and this means that spine synapses may appear more elaborate than those commonly found on the dendritic shaft. Although the significance of these differences in shapes and sizes has yet to be elucidated, experiments in hippocampal slice cultures indicate that larger excitatory postsynaptic current (EPSCs) are correlated with larger postsynaptic densities (Schikorsky and Stevens, 1997), so the measurements of synaptic densities in neocortex may provide insights into the comparative efficacy of synapses originating in different pathways.

The difference in the target neurons between layer 4 and layer 3 was unusual. From our evidence, only the V2 projection to layer 4 forms synapses with smooth (putative GABAergic) neurons, which were about 10% of the targets. The V2 projection to the superficial layers formed synapses exclusively with spiny neurons. We noted a similar trend, albeit not quite so marked in the projection of V2 to MT, in which 15% of the targets in layer 4 were smooth neurons, whereas, in layer 3, only 8% of the targets were smooth neurons. This raises the question of whether the same set of fibers provides this differential input to the two layers. From our data, it seems that single fibers do span the layer 3–4 border, but, in general, too many fibers were labeled to be able to trace any single fiber over several sections. Thus, we cannot be sure that there is not a population that arborizes exclusively in layer 3, as seems to be the case in the projection from V1 to V2 (Rockland and Virga, 1990). One additional difference between layer 3 and layer 4 was that, in layer 4, five of the target spines formed a second synapse with an unlabeled bouton. The second synapse was always symmetric. We had observed this same configuration in the context of the thalamic input to cortex (Dehay et al., 1991). Despite the fact that spines were the exclusive target in layer 3, we found no dual-input spines.

Physiological studies of macaqueV3A indicate that the neurons are not color sensitive (Zeki, 1978a) and that, compared with the case in MT, the proportion of direction-selective neurons is low (Zeki, 1978a; Galletti et al., 1990). Nevertheless, behavioral studies show that there are neurons in V3A sensitive to eye position (Galletti and Battaglini, 1989; Nakamura and Colby, 2000, 2002). Attention and expectation of reward in a task involving motion judgments modulate the responses of V3A neurons (Thiele et al., 1999; Nakamura and Colby, 2000). Thus, one view of V3A is that it forms a component of a visuosomatomotor pathway to the premotor cortex (Shipp et al., 1998). However, given the anatomical evidence of V3A's connections to the inferotemporal cortex and the physiological evidence from Gaska et al. (1988) that the temporal frequency tuning was low-pass, both the input and the output from V3A might be more heterogeneous than the traditional divisions into dorsal and ventral processing streams would imply. Given the anatomical and functional segregation of V2 (DeYoe and Van Essen, 1985; Shipp and Zeki, 1985; Hubel and Livingstone, 1987; Ts'o et al., 2001), it would be interesting to know which subdivisions of V2 provide the input to V3A.

ACKNOWLEDGMENTS

We thank German Koestinger and Nuno da Costa for their expert assistance.

LITERATURE CITED

Adams DL, Zeki S. 2001. Functional organization of macaque V3 for stereoscopic depth. J Neurophysiol 46:2195–2203.

Ahmed B, Anderson JC, Martin KAC, Nelson JC. 1997. Map of the synapses onto layer 4 basket cells of the primary visual cortex of the cat. J Comp Neurol 380:230–242.

Andersen RA, Asanuma C, Essick G, Siegel RM. 1990. Corticocortical connections of anatomically and physiologically defined subdivisions within the inferior parietal lobule. J Comp Neurol 296:65–113.

Anderson JC, Martin KAC. 2002. Connection from cortical area V2 to MT in macaque monkey. J Comp Neurol 443:56–70.

Anderson JC, Binzegger T, Martin KAC, Rockland KS. 1998. The connection from cortical area V1 to V5: a light and electron microscopic study. J Neurosci 18:10525–10540.

Backus BT, Fleet DJ, Parker AJ, Heeger DJ. 2001. Human cortical activity correlates with stereoscopic depth perception. J Neurophysiol 86:2054–2068.

Baizer JS, Ungerleider LG, Desimone R. 1991. Organization of visual inputs to the inferior temporal and posterior parietal cortex in macaques. J Neurosci 11:168–190.

Beck PD, Kaas JH. 1999. Cortical connections of the dorsomedial visual areas in the Old World macaque monkey. J Comp Neurol 406:487–502.

Blatt GJ, Andersen RA, Stoner GR. 1990. Visual receptive field organization and cortico-cortical connection of the lateral intraparietal area (area LIP) in the macaque. J Comp Neurol 299:421–445.

Boussaoud D, Ungerleider LG, Desimone R. 1990. Pathways for motion analysis: cortical connections of the medial superior temporal and fundus of the superior temporal visual areas in the macaque. J Comp Neurol 296:462–495.

Cavada C, Goldman-Rakic PS. 1989. Posterior parietal cortex in rhesus monkey. I. Parcellation of areas based on distinctive limbic and sensory corticocortical connections. J Comp Neurol 287:393–421.

Colby CL, Gattass R, Olson CR, Gross CG. 1988. Topographical organization of cortical afferents to extrastriate visual area PO in the macaque: a dual tracer study. J Comp Neurol 269:392–413.

Dehay C, Douglas RJ, Martin KAC, Nelson JC. 1991. Excitation by geniculocortical synapses is not "vetoed" at the level of dendritic spines in cat visual cortex. J Physiol 440:723–734.

DeYoe EA, Van Essen DC. 1985. Segregation of efferent connections and receptive field properties in visual area V2 of the macaque. Nature 317:58–61.

Felleman DJ, Van Essen DC. 1983. The connection of area V4 of macaque monkey extrastriate cortex. Soc Neurosci Abstr 9:153.

Felleman DJ, Burkhalter A, Van Essen DC. 1997. Cortical connections of areas V3 and VP of macaque extrastriate visual cortex. J Comp Neurol 379:21–47.

Galletti C, Battaglini PP. 1989. Gaze-dependent visual neurons in area V3a of monkey prestriate cortex. J Neurosci 9:1112–1125.

Galletti C, Battaglini PP, Fattori P. 1990. "Real-motion" cells in area V3A of macaque visual cortex. Exp Brain Res 82:67–76.

Gaska JP, Jacobson LD, Pollen DA. 1988. Spatial and temporal frequency selectivity of neurons in visual cortical area V3a of the macaque monkey. Vis Res 28:1179–1191.

Gattass R, Sousa APB, Mishkin M, Ungerleider LG. 1997. Cortical projections of area V2 in the macaque. Cereb Cortex 7:1047–3211.

Girard P, Salin PA, Bullier J. 1991. Visual activity in areas V3a and V3 during reversible inactivation of area V1 in the monkey. J Neurophysiol 66:1493–1503.

Hubel DH, Livingstone MS. 1987. Segregation of form, colour, and stereopsis in primate area 18. J Neurosci 7:3378–3415.

Kennedy H, Bullier J. 1985. Double-labeling investigation of the afferent connectivity to cortical areas V1 and V2 of the macaque monkey. J Neurosci 10:2815–2830.

Kisvárday ZF, Martin KAC, Whitteridge D, Somogyi P. 1985. Synaptic connections of intracellularly filled clutch neurons, a type of small basket neuron in the visual cortex of the cat. J Comp Neurol 241:111–137.

Latawiec D, Martin KAC, Meskenaite V. 2000. Termination of the geniculocortical projection in the striate cortex of macaque monkey: a quantitative immunoelectron microscopic study. J Comp Neurol 419:306–319.

Morel A, Bullier J. 1990. Anatomical segregation of two cortical visual pathways in the macaque monkey. Vis Neurosci 4:555–578.

Nakamura H, Kuroda T, Wakita M, Kato A, Mikami A, Sakata H, Itoh K. 2001. From three-dimensional space vision to prehensile hand movements: The lateral intraparietal area links the area V3a and the anterior intraparietal area in macaques. J Neurosci 21:8174–8187.

Nakamura K, Colby CL. 2000. Visual, saccade-related, and cognitive activation of single neurons in monkey extrastriate area V3a. J Neurophysiol 84:677–692.

Nakamura K, Colby CL. 2002. Updating of the visual representation in monkey striate and extrastriate cortex during saccades. Proc Natl Acad Sci U S A 99:4026–4031.

Orban GA, Fize D, Hendrik P, Denys K, Nelissen K, Sunaert S, Todd J, Vanduffel W. 2003. Similarities and differences in motion processing between the human and macaque brain: evidence from fMRI. Neuropsychologia 41:1757–1768.

Peters A, Saint Marie RL. 1984. Smooth and sparsely spinous nonpyramidal cells forming local axonal plexuses. In: Jones EG, Peters A, editors. Cerebral cortex, vol 1. Cellular components of the cerebral cortex. New York: Plenum Press. p 419–445.

Peters A, Palay SL, Webster HDeF. 1991. The fine structure of the nervous system: neurons and their supporting cells, 3rd ed. Oxford: Oxford University Press.

Rockland KS, Virga A. 1990. Organization of individual cortical axons projecting from area V1 (area 17) to V2 (area 18) in the macaque monkey. Vis Neurosci 4:11–28.

Rockland KS, Andresen J, Cowie RJ, Robinson DL. 1999. Single axon analysis of pulvinocortical connections to several visual areas in the macaque. J Comp Neurol 406:221–250.

Schall JD, Morel A, King DJ, Bullier J. 1995. Topography of visual cortex connections with frontal eye field in macaque: convergence and segregation of processing streams. J Neurosci 15:4464–4487.

Schikorski T, Stevens CF. 1997. Quantitative ultrastructural analysis of hippocampal excitatory synapses. J Neurosci 17:5858–5867.

Shipp S, Zeki S. 1985. Segregation of pathways leading from area V2 to areas V4 and V5 of macaque monkey visual cortex. Nature 315:322–325.

Shipp S, Blanton M, Zeki S. 1998. A visuo-somatomotor pathway through superior parietal cortex in the macaque monkey: cortical connections of areas V6 and V6a. Eur J Neurosci 10:3171–3193.

Somogyi P, Kisvárday ZF, Martin KAC, Whitteridge D. 1983 Synaptic connections of morphologically identified and physiologically characterised large basket cells in the striate cortex of cat. Neuroscience 10:261–294.

Stanton GB, Bruce CJ, Goldberg ME. 1995. Topography of projections to posterior cortical areas from the macaque frontal eye fields. J Comp Neurol 353:291–305.

Sterio DC. 1984. The unbiased estimation of number and sizes of arbitrary particles using the disector. J Microsc 134:127–136.

Thiele A, Distler C, Hoffmann KP. 1999. Decision-related activity in the macaque dorsal visual pathway. Eur J Neurosci 11:2044–2058.

Tootell RBH, Mendola JD, Hadjikhani NK, Leddon PJ, Liu AK, Reppas JB, Sereno MI, Dale AM. 1997. Functional analysis of V3a and related areas in human visual cortex. J Neurosci 17:7060–7078.

Tsao DY, Vanduffel W, Sasaki Y, Fize D, Knutson TA, Mandeville JB, Wald LL, Dale AM, Rosen BR, Van Essen DC, Livingstone MS, Orban GA, Tootell RBH. 2003. Stereopsis activates V3a and caudal intraparietal areas in macaques and humans. Neuron 39:555–568.

Ts'o DY, Wang Roe A, Gilbert CD. 2001. A hierarchy of the functional organization for color, form and disparity in primate visual area V2. Vis Res 41:1333–1349.

Van Essen DC, Newsome WT, Maunsell JH, Bixby JL. 1986. The projections from striate cortex (V1) to areas V2 and V3 in the macaque monkey: asymmetries, areal boundaries, and patchy connections. J Comp Neurol 244:451–480.

Webster MJ, Bachevalier J, Ungerleider LG. 1994. Connections of inferior temporal areas TEO and TE with parietal and frontal cortex in macaque monkeys. Cereb Cortex 4:470–483.

Zeki SM. 1978a. Uniformity and diversity of structure and function in the rhesus monkey prestriate visual cortex. J Physiol 277:273–290.

Zeki SM. 1978b. The cortical projections of foveal striate cortex in the rhesus monkey. J Physiol 277:227–244.